Available online at www.sciencedirect.com

SciVerse ScienceDirect

Ceramics International 39 (2013) 1257–1263

CERAMICS INTERNATIONAL

www.elsevier.com/locate/ceramint

Possible use of waste olivine powders from a foundry process into the ceramic industry: Sintering behaviour of olivine, kaolin and their blends

E. Furlani*, G. Tonello, E. Aneggi, S. Maschio

Università di Udine, Dipartimento di Chimica, Fisica e Ambiente, Via del Cotonificio 108, 33100 Udine, Italy

Received 31 May 2012; received in revised form 27 June 2012; accepted 17 July 2012
Available online 24 July 2012

Abstract

The present basic research aims to evaluate the possible recycling of olivine, a by-product of a foundry process, into the ceramic industry. With this goal in mind, olivine powders (*O*) were milled alone or blended with 20, 40, 60 and 80 wt% of a high grade kaolin (*K*) by attrition milling to obtain powders of different composition. Samples made with *K* alone were also prepared as blank composition. All mixtures were dried, sieved, uniaxially pressed into specimens and air sintered for 1 h at temperatures ranging from 1100 to 1400 °C. The resulting materials were characterized by water absorption, shrinkage and phase composition in order to test their sintering behaviour. It was observed that all compositions, sintered below 1100 °C display high open porosity, but enter into the final sintering stages between 1150 and 1200 °C as a function of their compositions, when their water absorption lowers below 5%.

Keywords: Olivine; Kaolin; Sintering; Traditional ceramics

1. Introduction

Foundry sand is a natural raw material used by foundries to create molds or cores particularly for casting iron based alloys. The criteria for foundry sand selection vary with the type of casting process employed by a given foundry (i.e., type of alloys produced) and include refractoriness, permeability, bond strength, grain fineness and chemical reactivity which are determined by grain shape, grain size, clay and moisture content and others.

Ideal foundry sands are generally subangular in shape which allows individual grains to interlock and form good molds while providing necessary pore spaces for superheated gases to escape without breaking the mold during the casting process. Grain size affect mold permeability and the finish of the casted part. A suitable grain size distribution for foundry sand is centred on U.S. Standard Sieve 70 (212 μm), with very little sand being retained on sieve sizes lower than 30 (590 μm) or greater than 140 (105 μm). It follows that any commercial sand supplied to a foundry and there stored, must be de-pulverized before its use for molds preparation in order to cut off its finest fraction. This fine sand part turns into a by product, although not a real waste, and needs to be used as raw material in any other production process rather than an eventual landfill disposal.

Foundries generally use high quality quartz sands for their molding preparations which are of a higher quality with respect to the typical bank run or natural sands used in fill construction sites; their finest fraction, cut off by the de-pulverization process, is presently used for the production of special cements [1–3], additional component for concretes [4,5] or starting material for glass or other ceramics preparation [6,7] and others [8–10].

On the other hand, for the production of manganese containing steels parts, it has been demonstrated that quartz sand needs to be replaced by *O* sand in order to reduce the reaction between quartz particles and the metal

*Corresponding author. Tel.: +39 432 558877; fax: +39 432 558803.
E-mail addresses: erika.furlani@uniud.it (E. Furlani), gabriele.tonello@uniud.it (G. Tonello), eleonora.aneggi@uniud.it (E. Aneggi), stef.maschio@uniud.it (S. Maschio).

0272-8842/$ - see front matter © 2012 Elsevier Ltd and Techna Group S.r.l. All rights reserved.
http://dx.doi.org/10.1016/j.ceramint.2012.07.056

under casting [11]; also *O* sands must display a restricted grain size distribution because particles must fall into a range of acceptable values and therefore must be de-pulverized before its use in molds preparation. *O* fine powder is therefore a non ordinary by product which would require a possible valuable application as component raw material of another production process.

Concerning quartz sands, many papers document their use as component for the production of some ceramic wares [12,13], conversely, the use of Mg containing silicates such as forsterite or cordierite is widely documented [14–17], but that of olivine or olivine containing powders is presently confined to the production of some special refractory bricks [18,19] or particular glazes for tiles [20].

The aim of present research is to study the sintering behaviour of *O* fine powders alone or mixed, in different proportions, with a high grade *K* in order to evaluate its possible recycling into the production of ceramic materials. With this goal in mind, powders of each composition, pressed into several specimens, were fired at different temperatures for 1 h, then shrinkage and water absorption were measured in order to build up their sintering curves; crystal phases were investigated as a function of the sintering cycle.

2. Materials and methods

The *O* powder used in the present work is a by product of a foundry process devoted to the production of a high manganese steel. Before molds preparation, *O* sand needs to be de-pulverized in order to cut off particles with size below 20 μm. The resulting *O* powder was used, in the present research, alone or blended with 20, 40, 60 and 80 wt% of a high grade *K*. Samples made with *K* alone were also prepared as reference composition. Symbols used for samples identification are, respectively *O*, OK20, OK40, OK60, OK80 and *K*.

The particle size distribution (PSD) of the as received *O* and *K* powders are reported in Fig. 1 which also displays that of a blend after the attrition milling process.

The chemical composition of the above raw materials, obtained by a Spectro Mass 2000 induced coupled plasma (ICP) mass spectrometer, is reported in Table 1 which also displays lost on ignition (LOI) after a thermal treatment at 1000 °C for 2 h.

O alone, *K* alone and all the blends (70 g of powder for each preparation) were homogenized by attrition milling for 1 h in a home made instrument. Milling parameters are as follows: high-density nylon container (volume = 750 ml); 500 g of 99 wt% alumina balls (diameter = 6–8 mm); 150 ml of distilled water; 300 cycles min^{-1}. At the end of the milling process, slurries were oven dried for 24 h at 80 °C. After milling, PSD was evaluated using a Horiba LA950 laser scattering PSD analyzer: analyses were made in water after a 3 min sonication time. For clarity of comprehension PSD curves are represented with logarithmic abscissa, as it is commonly done for the presentation of this type of results. Dried powders were sieved (200 μm–70 mesh) and uniaxially pressed at 100 MPa into cylindrical specimens ($\Phi = 27$ mm, $h = 4.5$ mm). Density of green samples was determined by the ratio between weight and volume which was evaluated by a caliper. Reported data are averaged over three measurements. Sintering experiments were performed in air, by an electric muffle, at several temperatures ranging from 1100 to 1350 °C with intervals of 50 °C using heating and cooling rates of 10 °C min^{-1} and a dwell time of 1 h.

Shrinkage on firing was evaluated, by a caliper, along the diameter (27 mm on green specimens) using the ratio $(\Phi_0 - \Phi_1)/\Phi_0$ (subscripts 0 and 1 refer to the sample dimensions before and after the sintering), whereas water absorption was determined following the norm EN99; in line with this norm, fired samples were first weighed in air (W_1), then placed in a covered beaker and boiled in

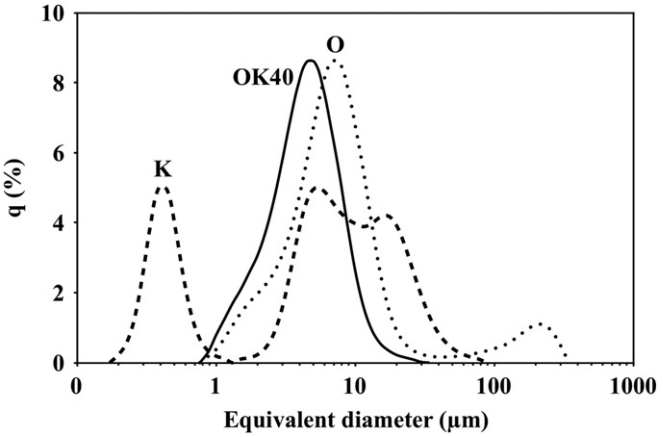

Fig. 1. Particle size distribution of the as received olivine (*O*) and kaolin (*K*) powders and that of the blend OK40 after the attrition milling process. Curves are represented with logarithmic abscissa.

Table 1
Composition (wt%) and LOI (%) of kaolin (*K*) and olivine (*O*) used as starting materials in the present study.

Component	Kaolin	Olivine
SiO_2	47.20	41.35
Al_2O_3	36.84	0.96
CaO	0.05	1.08
MgO	0.09	45.65
Na_2O	0.08	< 0.01
K_2O	1.10	< 0.01
Fe_2O_3	0.34	–
FeO	–	6.61
Cr_2O_3	< 0.01	0.19
TiO_2	0.31	< 0.01
NiO	< 0.01	0.27
MnO	< 0.01	0.06
P_2O_5	0.28	< 0.01
$SO_4^{=}$	0.08	< 0.01
Cl^-	0.14	< 0.01
Undetermined	1.19	0.73
LOI	12.30	3.10

water for 2 h. After boiling, samples were cooled in water to room temperature, dried with a cloth and weighed again (W_2). Water absorption was evaluated using the formula: $W(\%)=100[(W_2-W_1)/W_1]$.

Crystal phases were investigated by X-ray diffraction (XRD); XRD patterns were recorded on a Philips X'Pert diffractometer operated at 40 kV and 40 mA using Ni-filtered Cu-K_α radiation. Spectra were collected using a step size of 0.02° and a counting time of 15 s per angular abscissa in the range 10–80°. The Philips X'Pert HighScore software was used for phase identification.

3. Results

The chemical analysis of *K* revealed the presence of high quantities of SiO_2, Al_2O_3 and minor fractions of other components in line with literature data [21,22] as is its LOI value; on the other hand, *O* contains high quantities of SiO_2, MgO, Fe_2O_3, minor quantities of Al_2O_3, CaO and small fractions of NiO, Cr_2O_3 and MnO.

Fig. 1 shows the PSD curves of the as received materials and that of the blend OK40 which was selected as an example of all powder after the milling procedure. It can be observed that *O* displays a bimodal PSD which shows great peak centred on 7 μm and one, smaller, centred on 200 μm thus showing that the upstream de-pulverization process is sufficiently efficient in its task. *K* shows a scattered PSD with three great peaks: one centred on 400 nm, the second on 5 μm and the third close to 20 μm. The curve representative of the blend OK40 shows a monomodal PSD with a great peak centred on 5 μm and demonstrates that the attrition milling procedure makes uniform the PSD of the mixture. All the other blends, after the milling procedure, displayed PSD curves very close to that of OK40, however they are not displayed in Fig. 1 in a cumulative graphic in order to avoid confusion by the reader. Anyway, as a consequence of the milling procedure, it was assumed that PSD have same effect on the resulting sintered compositions.

The XRD investigation (Fig. 2) revealed that *O* powder mainly contains forsterite (PDF 01-079-1210) with enstatite (PDF 00-019-0768) and quartz (PDF 01-083-2465) as minor phases, whereas kaolinite (PDF 00-029-1488) and a small quantity of free quartz were detected in *K*.

Below are reported the sintering trends of the materials prepared in the present work: comments take account of the phases development observed by the XRD analysis. For an easier comprehension, the next part of the present section is divided into three subsections each one containing description and discussion of the results obtained on materials displaying similar sintering curves.

3.1. Compositions O and K

Fig. 3 reports shrinkage and water absorption trends as a function of the firing cycle of samples made with *O* and *K* alone whereas Fig. 4a and b reports the XRD patterns of

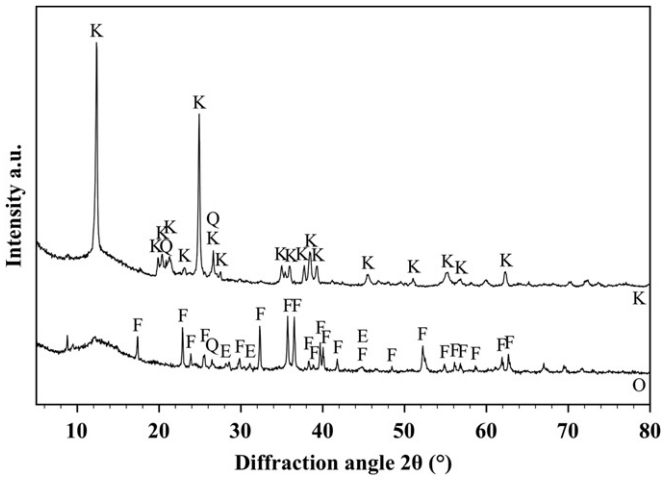

Fig. 2. X-ray diffraction patterns of the as received *O* and *K* powders. Phases are identified by the following symbols: (*E*)=enstatite; (*F*)=forsterite; (*Q*)=quartz and (*K*)=kaolinite.

the two compositions after sintering cycles at 1100, 1200 and 1300 °C, respectively. During the experimental work, it has been observed that the samples made with *O*, when fired at temperatures greater than 1300 °C, progressively soften and loose their shape (due to the formation of a high amount of liquid phase): shrinkage cannot be clearly determined so that the corresponding curves end at 1300 °C.

Conversely, specimens made with *K* may be fired up to 1450 °C, but no significative shrinkage, water absorption and phase changes were observed above 1300 °C. It can be observed that *O* and *K* have similar trends in all the range investigated, even if the final sintering temperature greatly affect shrinkage and water absorption of the fired materials. Fig. 4a shows that samples made with *O* contain enstatite and forsterite at any sintering temperature. As a consequence, the huge change of shrinkage and water absorption which is observed between 1150 and 1250 °C is probably related to the formation of a certain quantity of liquid phase which becomes greater and greater with increasing firing temperature. Fig. 4b shows that, at 1100 °C, samples made with *K* still contain a certain amount of the original quartz, mullite (PDF 00-010-0394) and a silica rich glassy phase revealed by the non flat profile of the background line; same phases were detected after the cycle at 1200 °C, but the amount of mullite increases; the firing cycle at 1300 °C causes a further increase of mullite and amorphous phase, whereas quartz transforms into tridimite (PDF 01-076-0894) and cristobalite (PDF 01-085-0621). Materials fired at higher temperatures show the presence of same phases as after the cycle at 1300 °C.

3.2. Compositions OK20 and OK40

Fig. 5 shows shrinkage and water absorption trends as a function of the firing cycle of compositions OK20 and OK40; as it was observed testing samples made with *O* alone, also these two compositions, when fired at temperatures greater

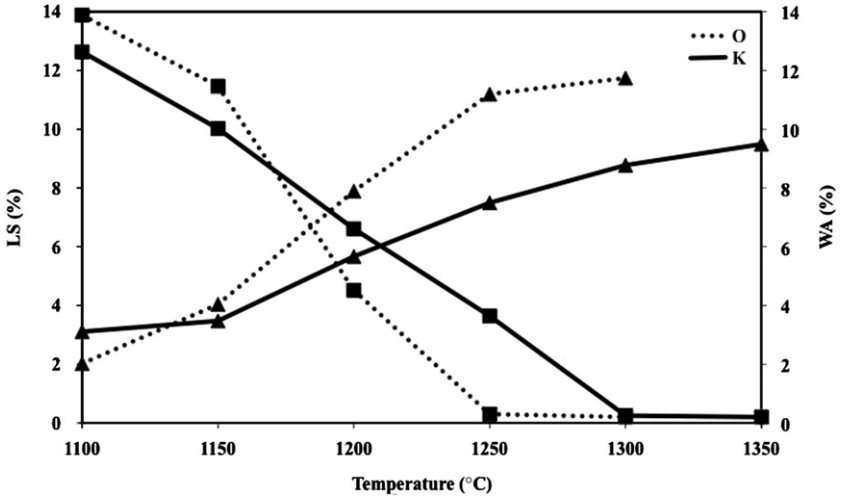

Fig. 3. Linear shrinkage (LS) and water absorption (WA), as a function of firing temperature of samples made of *O* and *K* alone (LS: ♦ WA: ■).

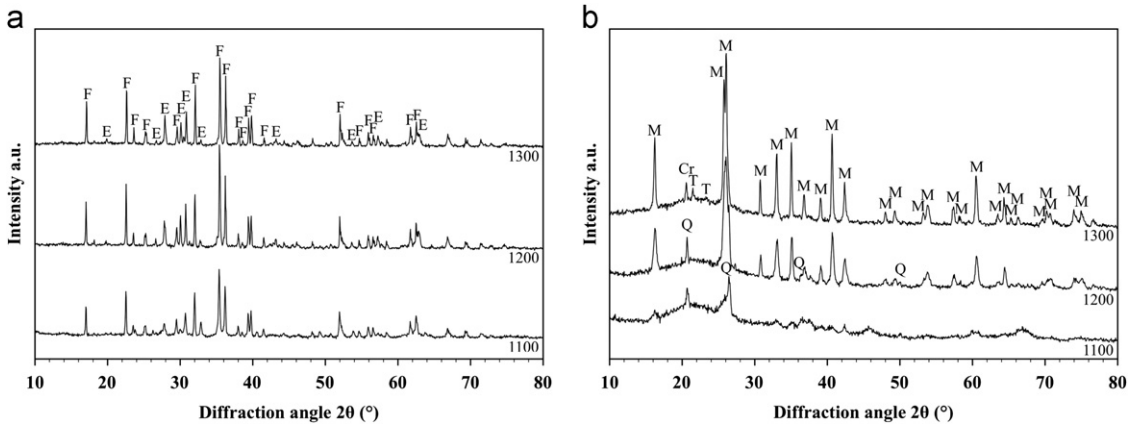

Fig. 4. X-ray diffraction patterns between 10° and 80° acquired on the free surface of samples *O* (a) and *K* (b) fired at 1100, 1200 and 1300 °C. Phases are identified by the following symbols: (*E*)=enstatite; (*F*)=forsterite; (*M*)=mullite; (*Cr*)=cristobalite; (*T*)=tridimite and (*Q*)=quartz.

than 1300 °C, progressively soften and loose their shape (formation of huge quantities of liquid phase): in this case, as well, shrinkage cannot be clearly determined so that the corresponding trends are stopped there.

It can be also observed that, for both compositions, water absorption reaches the lowest values after firing cycles with top temperatures equal or greater than 1200 °C. At the same time, shrinkage is maximum after the cycle at 1200 °C, but higher top temperatures cause a reduction of shrinkage. This particular phenomenon can be much more clearly understood if are observed Fig. 6a and b which show the XRD patterns of the two compositions after sintering cycles at 1100, 1200 and 1300 °C, respectively. It can be seen that, at 1100 °C, forsterite, mullite and cristobalite are present in OK20 whereas fosterite, mullite and enstatite are present in OK40. However, first the nucleation and then a rapid growth of the amount of cordierite (PDF 01-083-1597) can be observed when both materials are fired at temperatures equal or greater than 1200 °C. The amount of cordierite runs inversely proportional to that of forsterite which completely disappears after firing at 1300 °C. The theoretical density of cordierite is 2.50 g cm^{-3} and is lower than that of forsterite (3.70 g cm^{-3}). Theoretical density shows that the crystal structure of forsterite is much more densely packed with respect to cordierite crystals: it follows that materials where cordierite replaces forsterite may display low water absorption (low open porosity), but shrinkage, after the firing cycle, is lower with respect to samples fired at lower temperatures. The above described phenomenon could be amplified by a possible overfiring effect typically enhanced by the presence of MgO which could cause de-sintering and eventually bloating [23].

3.3. Compositions OK60 and OK80

Same considerations regarding the top firing temperature as those made about most of the compositions discussed above could be done also for OK60 and OK80 materials which, due to the formation of a huge quantity liquid phase, do not enable shrinkage evaluation when fired at temperatures higher

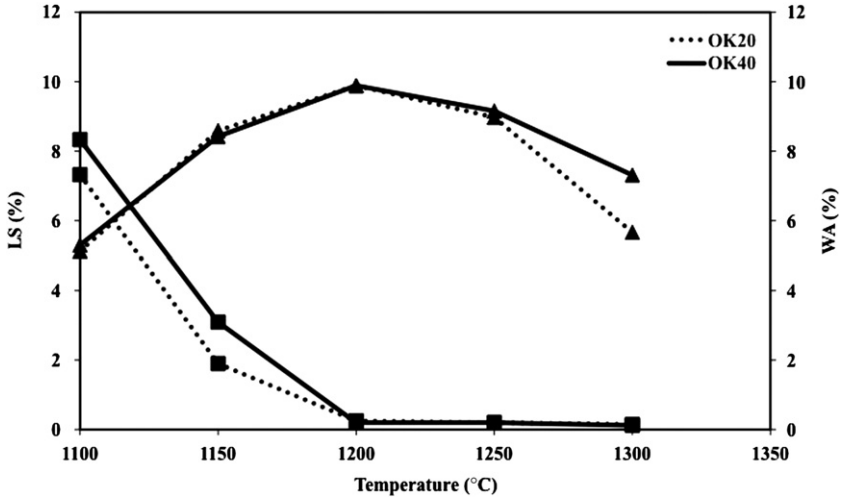

Fig. 5. Linear shrinkage (LS) and water absorption (WA), as a function of firing temperature, of samples OK20 and OK40 (LS: ♦; WA: ■).

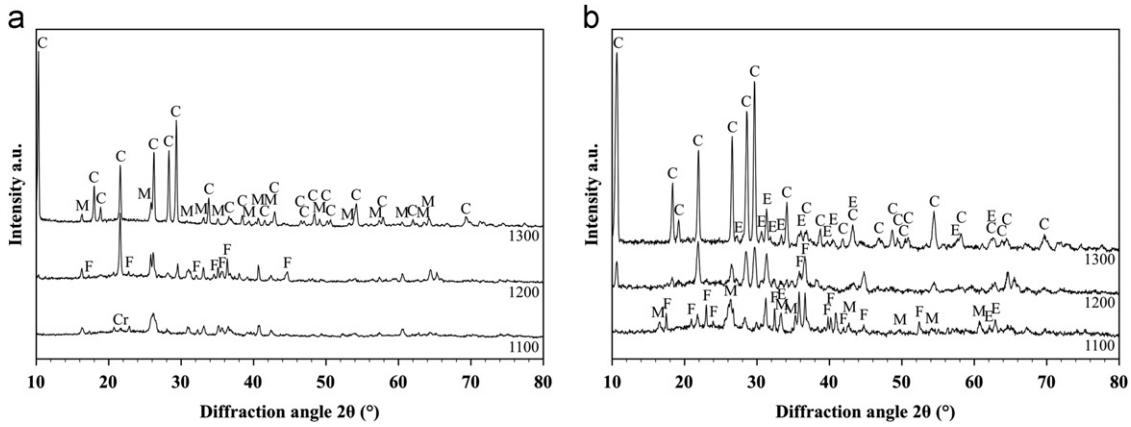

Fig. 6. X-ray diffraction patterns between 10° and 80° acquired on the free surface of samples OK20 (a) and OK40 (b) fired at 1100, 1200 and 1300 °C. Phases are identified by the following symbols: (*C*)=cordierite; (*M*)=mullite; (*F*)=forsterite; (*Cr*)=cristobalite and (*E*)=enstatite.

than 1300 °C thus their corresponding sintering curves are stopped there. OK60 has water absorption around 10% after a firing cycle at 1100 °C (see Fig. 7), but this value rapidly decreases when samples are fired at higher temperatures and is reduced below 2% when samples are fired at temperatures greater than 1200 °C. At the same time its shrinkage grows rapidly between 1100 and 1200 °C, but thereafter remains constant. Water absorption of OK80 is between 12 and 13% after firing cycles at 1100 °C, but, for higher temperatures, it rapidly decreases and reaches values close to zero when fired at temperatures greater than 1250 °C; the corresponding shrinkage increases continuously as temperature is increased up to 1250 °C, but for higher temperatures it remains constant.

Fig. 8a and b show the X-ray diffraction patterns of the two compositions after sintering cycles at 1100, 1200 and 1300 °C, respectively. It can be observed that, at 1100 °C, OK60 contains enstatite, forsterite and mullite (PDF 01-079-1453, different from that identified in *K* alone and OK20) which turns into cordierite, or perhaps into indialite which has crystal structure similar to that of cordierite, contains Fe^{2+} and has diffraction peaks at nearly same positions, for firing cycles at higher temperatures. Here also must be pointed out that the structure of mullite is more densely packed than that of cordierite (the theoretical density of mullite is 3.17 whereas that of cordierite is 2.50 g cm^{-3}) even if the difference is not so large as that between cordierite and forsterite. As a consequence materials with progressively reduced water absorption values could show constant shrinkage as it can be observed for samples with composition OK60 when fired at temperatures between 1200 and 1250 °C.

Fig. 8b shows that materials with composition OK80, when fired at 1100 °C, contain enstatite, forsterite and spinel (PDF 00-021-0540); for higher sintering temperatures, the peaks of enstatite and forsterite are well defined, as well as those of spinel which is enriched with Fe. For this composition, a flat trend of shrinkage is reached only after firing cycles at 1250 °C or above.

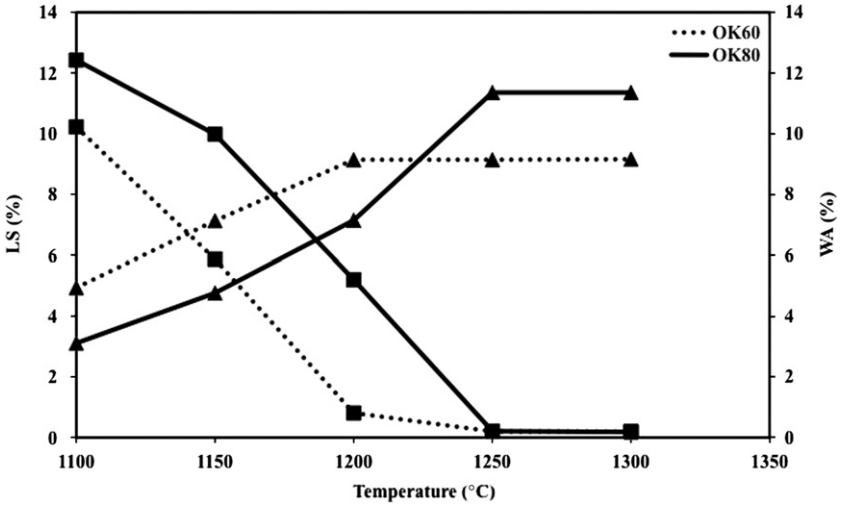

Fig. 7. Linear shrinkage (LS) and water absorption (WA), as a function of firing temperature, of samples OK60 and OK80 (LS: ♦; WA: ■).

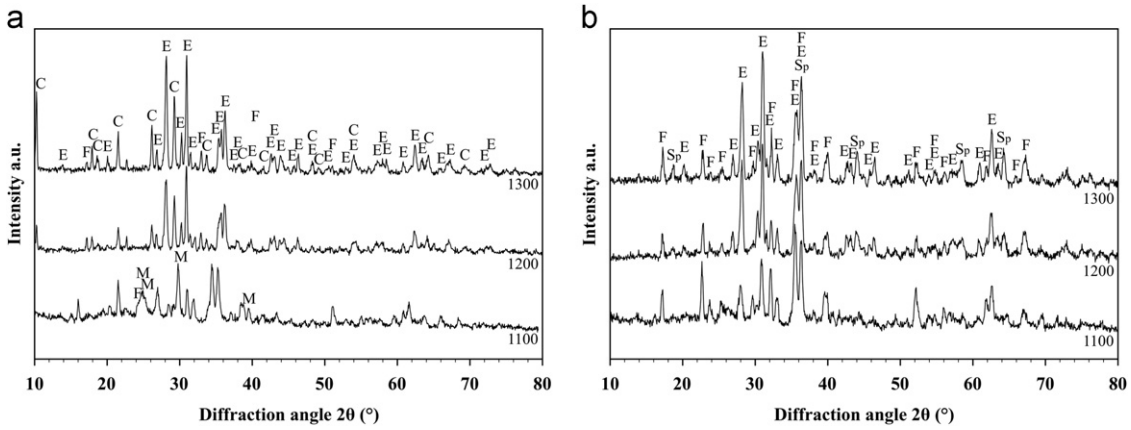

Fig. 8. X-ray diffraction patterns between 10° and 80° acquired on the free surface of samples OK60 (a) and OK80 (b) fired at 1100, 1200 and 1300 °C. Phases are identified by the following symbols: (*E*)=enstatite; (*F*)=forsterite; (*C*)=cordierite; (*M*)=mullite and (*Sp*)=spinel.

4. Discussion

All the materials prepared in the present research sinter in presence of liquid phase coupled with a rearrangement of their crystallographic structures; for such systems, Kingery [22] and then Shaw [24] have proposed sintering models that establish two steps for shrinkage: the first step shows a decrease in open porosity (coincident with a first increase of shrinkage), but the process does not finish when open porosity completely disappears, because in the second step, the ceramic body could be represented as a conjunction of small and closed pores; during this stage, the surface energy forces inside each pore give rise to a negative pressure, which tends to further densify the ceramic body. As temperature increases, the liquid phase, in addition to grains and crystal structures rearrangement, promotes particles disintegration, contributing to shrinkage and materials densification.

Based on this assumption and under a further detailed overview of the sintering trends discussed in the present paper, it is clear that all compositions, complete the first part of sintering process below 1100 °C and enter into the final stage between 1150 and 1200 °C when their water absorption (residual open porosity) lowers below 5%. At these temperatures shrinkage lowers the rate and materials shrinkage is virtually stopped, but grains continue to grow. These conditions are reached at different temperatures as a function of materials composition, being 1200 °C for OK20, OK40, OK60, and 1250 °C for *O* alone and OK80 and 1300 °C for *K* alone. In addition it is observed that samples made with *K* alone reach water absorption below 1% only when fired at temperatures equal or greater than 1300 °C; specimens of *O* alone or made with the blend OK80 reach similar values just after sintering at 1250 °C whereas all the other blends require a lower temperature (1200 °C). Such temperatures can be therefore assumed as upper limit in perspective of a possible production of materials with low open porosity, small grains and limited amount of amorphous phase such as, for example, porcelanized stoneware or earthenware tiles.

5. Conclusions

The present research deals with production and characterization of ceramics containing *O* powder deriving from a de-pulverizing foundry process devoted to the production of a high manganese steel and a natural *K*. *O*, *K* as well as their blends were mixed by wet attrition milling, dried, sieved, pressed into specimens and fired at several temperatures in the range 1100–1350 °C for 1 h.

The sintering experiments demonstrated that:

1. All compositions, complete the first part of sintering process (high open porosity) below 1100 °C and enter into the viscous sintering stage between 1150 and 1200 °C as a function of their compositions, when their water absorption lowers below 5%;
2. All compositions, except *K* alone, progressively soften and samples loose their shape, due to the presence of a high quantity of liquid phase when fired at temperatures higher then 1300 °C;
3. It is observed that samples made with the blend OK20, OK40 and OK60 reach water absorption below 1% when fired at temperatures equal or greater than 1200 °C; whereas all the other compositions require higher temperatures;
4. The XRD analysis of the fired samples revealed the presence of some phases already present in the starting components, however other phases grow during sintering and their quantity depends of the sintering cycle;
5. The materials fired at their optimal temperature could represent an option for a possible recycling of waste olivine into the production of tiles.

References

[1] O. Bonneau, C. Vernet, M. Moranville, P.-C. Aïtcin, Characterization of the granular packing and percolation threshold of reactive powder concrete, Cement and Concrete Research 30 (2000) 1861–1867.

[2] S.K. Agarwal, Pozzolanic activity of various siliceous materials, Cement and Concrete Research 36 (2006) 1735–1739.

[3] H. Justnes, P.A. Dahl, V. Ronin, J.-E. Jonasson, L. Elfgren, Microstructure and performance of energetically modified cement (EMC) with high filler content, Cement and Concrete Composites 29 (2007) 533–541.

[4] Q. Yang, S. Zhang, S. Huang, Y. He, Effect of ground quartz sand on properties of high-strength concrete in the steam-autoclaved curing, Cement and Concrete Research 30 (2000) 1993–1998.

[5] W.-Y. Kuo, J.-S. Huang, C.-H. Lin, Effects of organo-modified montmorillonite on strengths and permeability of cement mortars, Cement and Concrete Research 36 (2006) 886–895.

[6] Z.-J. Wang, W. Ni, Y. Jia, L.-P. Zhu, X.-Y. Huang, Crystallization behaviour of glass ceramics prepared from the mixture of nickel slag, blast furnace slag and quartz sand, Journal of Non-Crystalline Solids. 356 (2010) 1554–1558.

[7] J. Malaiskiene, R. Maciulaitis, A. Kicaite, Dependence of ceramics physical–mechanical properties on chemical and mineralogical composition, Construction and Building Materials 25 (2011) 3168–3174.

[8] G. Casalino, L.A.C. De Filippis, A. Ludovico, A technical note on the mechanical and physical characterization of selective laser sintered sand for rapid casting, Journal of Materials Processing Technology 166 (2005) 1–8.

[9] A. Pitois, L.G. Abrahamsen, P.I. Ivanov, N.D. Bryan, Humic acid sorption onto a quartz sand surface: a kinetic study and insight into fractionation, Journal of Colloid and Interface Science 325 (2008) 93–100.

[10] L. Hanchao, F. Suping, D. Xiaolin, Z. Nannan, L. Yongli, Comparison of three sorbents for organic pollutant removal in drinking water, Energy Procedia 5 (2011) 985–990.

[11] E.G. Davis, Beneficiation of Olivine Foundry Sand by Differential Attrition Grinding; US Patent no. 4039625 (1977).

[12] A. De Noni jr, D. Hotza, V. Cantavella Soler, E. Sanchez Vilches, Effect of quartz particle size on the mechanical behaviour of porcelain tiles subjected to different cooling rates, Journal of the European Ceramic Society 29 (2009) 1039–1046.

[13] S.R. Braganc, C.P. Bergmann, H. Hubner, Effect of quartz particle size on the strength of triaxial porcelain, Journal of the European Ceramic Society 26 (2006) 3761–3768.

[14] C.-M. Cheng, C.-F. Yang, S.-H. Lo, The influence of crystallization on the flexural strength of $MgO–CaO–Al_2O_3–SiO_2$, Ceramics International 25 (1999) 581–586.

[15] M.J. Ribeiro, J.A. Labrincha, Properties of sintered mullite and cordierite pressed bodies manufactured using Al-rich anodising sludge, Ceramics International 34 (2008) 593–597.

[16] N.T. Andrianov, S.S. Fedorova, S.M. Fedorova, S. Yu., Fedorova, the effect of initial components on the synthesis of forsterite produced by the sol–gel method, Glass and Ceramics 59 (2002) 199–202.

[17] L. Yu, H. Xiao, Y. Cheng, Influence of magnesia on the structure and properties of $MgO–Al_2O_3–SiO_2–F$—glass-ceramics, Ceramics International 62 (2008) 63–68.

[18] H. Palmour III, B. Gay, R.L. Cochrane, Olivine Refractory Bricks for Heat Storage Applications, US Patent no. 4303448 (1981).

[19] V.M. Goldschmidt, Olivine and forsterite refractories in Europe, Industrial and Engineering Chemistry 30 (1938) 32–34.

[20] M. Schabbach, F. Andreola, I. Lancellotti, L. Barbieri, Minimization of Pb content in a ceramic glaze by reformulation the composition with secondary raw materials, Ceramics International 37 (2011) 1367–1375.

[21] T. Manfredini, G.C. Pellacani, Engineering materials handbook, Ceramics and Glasses-ASTM (1992) 925–929.

[22] W.D. Kingery, Introduction to Ceramics, John Wiley and Sons Inc, New York, 1976.

[23] M.N. Rahaman, Ceramic, Processing and Sintering, second ed., Marcel Dekker, New York, 2003.

[24] T.M. Shaw, Liquid redistribution during liquid-phase sintering, Journal of the American Ceramic Society 69 (1986) 27–34.